Factors Controlling the Near-Surface Wind Field in Antarctica*

M. R. VAN DEN BROEKE

Institute for Marine and Atmospheric Research, Utrecht University, Utrecht, Netherlands

N. P. M. VAN LIPZIG+

Royal Netherlands Meteorological Institute, de Bilt, Netherlands

(Manuscript received 10 September 2001, in final form 27 April 2002)

ABSTRACT

Using data from the regional atmospheric climate model RACMO/ANT1 the momentum budget of the Antarctic atmospheric surface layer (SL; taken as the lowest model layer located at 6–7 m above the surface) is presented. In July (winter), the katabatic pressure gradient force (PGF) dominates the SL momentum budget over the steep coastal slopes, which results in strong (10–15 m s^{-1}) and directionally constant katabatic winds. Farther inland, where surface slopes are more gentle, the large-scale PGF may become equally important. With the circumpolar pressure trough north of the Antarctic coastline, the large-scale PGF acts along with the katabatic PGF in the downslope direction. In Wilkes Land, Dronning Maud Land, and on the western Ross Ice Shelf, the large-scale PGF causes equivalent geostrophic winds in excess of 10 m s^{-1}. Thermal wind effects that oppose the downslope acceleration are especially strong in areas where large-scale forcing is weak, which allows cold air to pile up over the flat ice shelves and sea ice–covered ocean. In January, absorption of shortwave radiation at the surface strongly reduces the katabatic forcing and thermal wind effects, and the large-scale PGF dominates the SL momentum budget. Interestingly, large-scale easterly winds in some regions are stronger in summer than in winter, which explains the year-round constancy of Antarctic SL winds. In contrast, the large-scale SL winds in coastal West Antarctica and the Antarctic Peninsula are very variable on the seasonal timescale.

1. Introduction

Antarctica is covered by the largest ice sheet on Earth (Fig. 1). It has a maximum elevation of over 4000 m and a volume equivalent to a global sea level rise exceeding 60 m. About half of the Antarctic coastline is fringed by 100–1000-m-thick, floating ice shelves, and for most of the year sea ice covers the surrounding oceans. The upper 70–100 m of the ice sheet consists of dry snow, with seasonal melting and runoff only occurring in the northernmost areas of the Antarctic Peninsula.

Two meteorological phenomena that are closely coupled characterize the Antarctic atmospheric surface layer (SL): a quasi-permanent temperature deficit (often described in terms of the temperature inversion strength, Phillpot and Zillman 1970; Connolley 1996) and the persistent low-level katabatic circulation (Parish and Bromwich 1987). During winter, in the absence of solar radiation, radiation losses cause the surface to become colder than the free atmosphere by as much as 30–35 K. Heat is then extracted from the overlying air through turbulent exchange, causing the SL air to cool and to become negatively buoyant with respect to the free atmosphere. The cold air that flows down the incline of the ice sheet represents the notorious Antarctic katabatic winds. Because the katabatic forcing is largest near the surface, where drag dominates, a wind speed maximum occurs at some height above the surface. The size of the continent and the persistent surface cooling in winter enables the Coriolis effect to deflect the katabatic winds in the cross-slope direction, but surface drag maintains a downslope component in a shallow layer below the wind speed maximum.

Many observational and modeling studies have been devoted to regional manifestations of Antarctic katabatic winds. Parish and Bromwich (1987) noted that channeling of air due to valley-shaped topography can locally enhance katabatic wind speeds. This is particularly true for Adélie Coast where the strongest winds on Earth are observed; the annual mean wind speed at

* European Project for Ice Coring in Antarctica Publication Number 59.

+ Current affiliation: British Antarctic Survey, Cambridge, United Kingdom.

Corresponding author address: Dr. M. R. van den Broeke, Institute for Marine and Atmospheric Research, Utrecht University, P.O. Box 80 005, 3508 TA Utrecht, Netherlands.
E-mail: broeke@phys.uu.nl

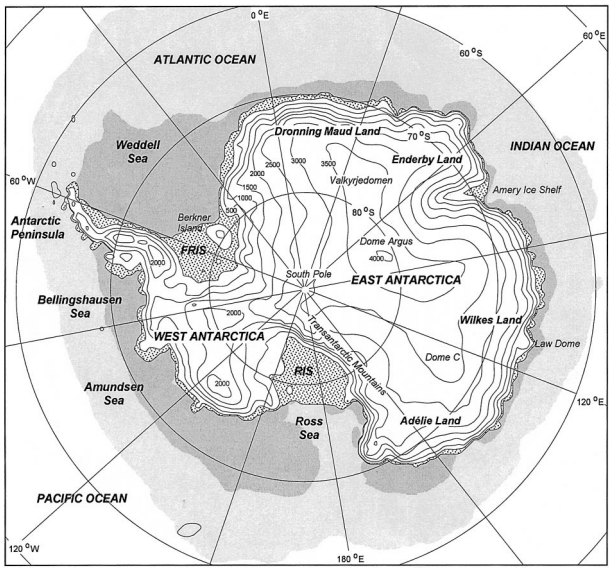

FIG. 1. Model domain and topographical features of Antarctica. Ice shelves (stippled); average Jul sea ice extent (light shaded); average January sea ice extent (dark shaded). Surface elevation (m MSL) is contoured every 500 m. RIS: Ross Ice Shelf; FRIS: Filchner–Ronne Ice Shelf.

Cape Denison was 19.4 m s^{-1} in 1912–13 (Schwerdtfeger 1970). Bromwich and Liu (1996) observed that air masses originating from West Antarctica flowed over colder katabatic air originating from the East Antarctic plateau.

A wide range of numerical models of Antarctic katabatic winds has been previously used for the study of Antarctic katabatic winds; high-resolution models [typically 10–20 km, 2D or 3D, Parish and Waight (1987), Gallée and Schayes (1992), Bromwich and Du (1994), Gallée et al. (1996)] as well as continental-scale simulations with regional models (e.g., Hines et al. 1995). Egger (1985) and James (1989) used idealized axisymmetric models to quantify the influence of the katabatic winds on the free tropospheric circulation. They found that the katabatic circulation sets up a cyclonic circulation in the free troposphere, but that without meridional export of angular momentum a katabatic circulation over Antarctica could not be maintained. A similar conclusion was reached by Parish (1992) using a 3D numerical model. General circulation models perform quite well over Antarctica nowadays (Genthon and Braun 1995; van den Broeke et al. 1997), but there are occasional problems with the representation of the surface (snow/ice shelves/sea ice, physical parameters of the subsurface material) and the resolution is seldom better than 100–150 km in the horizontal.

A question that has received much attention is how the large-scale pressure gradient force (PGF) and thermal wind effects in the boundary layer (caused by horizontal inhomogeneities) modify Antarctic katabatic winds. Weller (1969) and Kodama and Wendler (1986) noted that katabatic winds unexpectedly decrease near the coast, probably associated with an opposing pressure gradient force that may also be responsible for the occurrence of hydraulic jumps (Pettré and André 1991). Observations made by Kodama et al. (1989) showed that near-surface winds in coastal Adélie Land retain their high directional constancy in summer, in spite of the weak or absent katabatic PGF at solar noon. They showed that the large-scale temperature and wind field force near-surface winds that have a vertical structure very similar to that of the wintertime katabatic winds. More recently, Parish and Cassano (2001) used National Centers for Environmental Prediction–National Center for Atmospheric Research (NCEP–NCAR) reanalysis data in combination with Ball's (1960) theoretical bulk model of katabatic winds to partition the forces acting on the SL air for June/July/August 1997. They found a considerable influence of the large-scale PGF on the near-surface wind field. Van den Broeke et al. (2002) calculated vertical profiles of the momentum budget using data of a regional climate model. Both papers showed that the topography and physical characteristics of the East Antarctic ice sheet determine not only the structure of the SL but also the free troposphere temperature and wind fields.

In this paper we present the momentum budget of the SL to explain the near-surface wind field in Antarctica. In section 2 the model is briefly described. In section 3, we introduce the various terms in the SL momentum budget and how they are derived from model output. Section 4 presents the SL momentum budget for July, section 5 for January. A summary and a note on future work is given in section 6.

2. Model description and data analysis

The regional atmospheric climate model RACMO/ANT1 is based on the ECHAM4 model (van Lipzig 1999). The model domain of 122 × 130 grid points covers the entire Antarctica and part of the surrounding oceans (Fig. 1). At the lateral boundaries, RACMO is forced by ERA 15 data [European Centre for Medium-Range Weather Forecasts (ECMWF) reanalysis, 1980–93], which allowed for an uninterrupted 14-yr integration of the model. Horizontal resolution is approximately 55 km, which enables a reasonably accurate representation of the steep coastal ice slopes and the ice shelves fringing the coast. In the vertical, 20 hybrid levels are used. RACMO/ANT1 is a hydrostatic model. The assumption of hydrostatic balance is acceptable in katabatic flows as long as the horizontal length scales dominate the vertical ones (Mahrt 1982), as is usually the case in the Antarctic. Possible exceptions are nocturnal slope flows that develop in the Antarctic summer over local, steep topography (van den Broeke and Bintanja 1995). Compared to the original model version, several improvements were made with regard to the physical representation of the snow surface (albedo, spe-

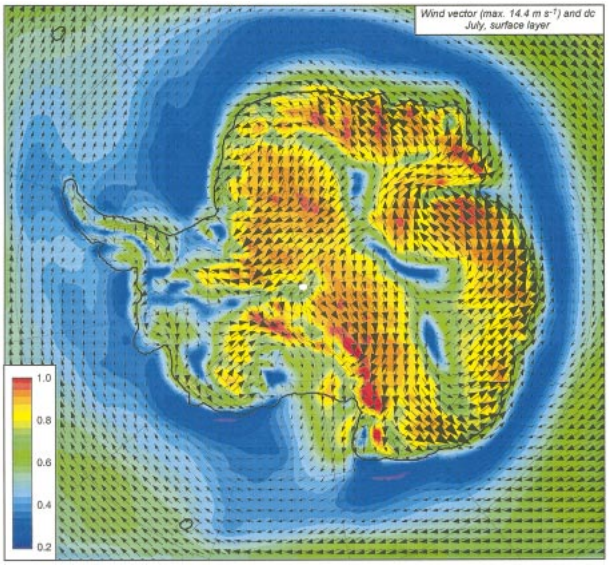

FIG. 2. Average Jul (1980–93) modeled SL wind vector (arrows) and directional constancy (colors).

cific heat and heat conductivity of the snow, deep snow temperature initialization). An additional layer at 7 m was included to better capture the strong temperature and wind speed gradients near the surface. This level is chosen to represent the SL.

Figure 2 shows the modeled July SL wind vector and directional constancy averaged over the period 1980–93. The directional constancy dc is defined as the ratio of the mean to vector mean wind speed:

$$\mathrm{dc} = \frac{(\overline{u}^2 + \overline{v}^2)^{1/2}}{\overline{(u^2 + v^2)^{1/2}}}. \tag{1}$$

The modeled SL wind velocities (9–14 m s^{-1}) and dc (0.9–0.95) are highest in the zone where the slope of the ice sheet is steepest, while weak winds and low dc are found over the domes of the interior ice sheet, in agreement with observations from manned and automatic weather stations (Allison et al. 1993). North of the Antarctic coastline, dc quickly decreases to attain a minimum value in the center of the circumpolar pressure trough (CPT), where transient eddies occur most frequently. North of the CPT, strong and persistent westerlies prevail near the surface.

In general, RACMO/ANT1 performance is a great improvement over earlier models (van Lipzig et al. 1998, 1999), but some problems remain. The surface roughness z_0 is composed of a basic value over snow (set to 1 mm) to which is added a contribution from subgrid topographical variance. The latter parameterization leads to overestimated z_0 and underestimated near-surface winds in regions of rough topography (e.g., the Transantarctic Mountains) and, because roughness lengths for heat and moisture z_h and z_q are set equal to z_0, overestimated turbulent exchange of heat and moisture.

3. The SL momentum budget: Definition and calculation method

a. Definition of the terms

The approximate equations for mean cross-slope (U) and downslope (V) flow on an inclined surface of constant slope α with coordinates (x, y, z) orthogonal to the surface (positive y directed down the slope, positive x directed to the right), can be written as

$$\underbrace{\frac{\partial U}{\partial t}}_{} = \underbrace{-U\frac{\partial U}{\partial x} - V\frac{\partial U}{\partial y}}_{\mathrm{ADVH}_c} \underbrace{- W\frac{\partial U}{\partial z}}_{\mathrm{ADVV}_c} + \underbrace{\frac{g}{\theta_0}\frac{\partial \hat{\theta}}{\partial x}}_{\mathrm{THW}_c} + \underbrace{fV}_{\mathrm{COR}_c} \underbrace{- fV_{\mathrm{LSC}}}_{\mathrm{LSC}_c} \underbrace{- \frac{\partial \overline{uw}}{\partial z}}_{\mathrm{FDIV}_c},$$

$$\underbrace{\frac{\partial V}{\partial t}}_{} = \underbrace{-U\frac{\partial V}{\partial x} - V\frac{\partial V}{\partial y}}_{\mathrm{ADVH}_d} \underbrace{- W\frac{\partial V}{\partial z}}_{\mathrm{ADVV}_d} + \underbrace{\frac{g}{\theta_0}\frac{\partial \hat{\theta}}{\partial y}}_{\mathrm{THW}_d} \underbrace{- fU}_{\mathrm{COR}_d} + \underbrace{fU_{\mathrm{LSC}}}_{\mathrm{LSC}_d} \underbrace{- \frac{\partial \overline{vw}}{\partial z}}_{\mathrm{FDIV}_d} + \underbrace{\frac{g}{\theta_0}\Delta_\theta \sin\alpha}_{\mathrm{KAT}},$$

$$\Delta_\theta(z) = \theta(z) - \theta_0(z); \qquad \hat{\theta}(z) = \int_z^{h_s+h} \Delta_\theta(z'')\, dz''. \tag{2}$$

The subscript LSC represents large-scale wind components, u, v, w are the components of the turbulent velocity fluctuations. Here, Δ_θ is the temperature perturbation of the SL air relative to the undisturbed background temperature θ_0. The value Δ_θ is obtained directly from an extrapolation procedure described later. The layer where Δ_θ is negative is defined as the temperature-deficit layer (TDL). Here, $\hat{\theta}$ (unit K m) is Δ_θ vertically integrated between height z and some height h that is chosen well above the top of the TDL; this way we avoid defining the depth of the stable atmospheric boundary layer, which is poorly constrained under stable conditions.

The subscripts c, d in Eq. (2) indicate down- and

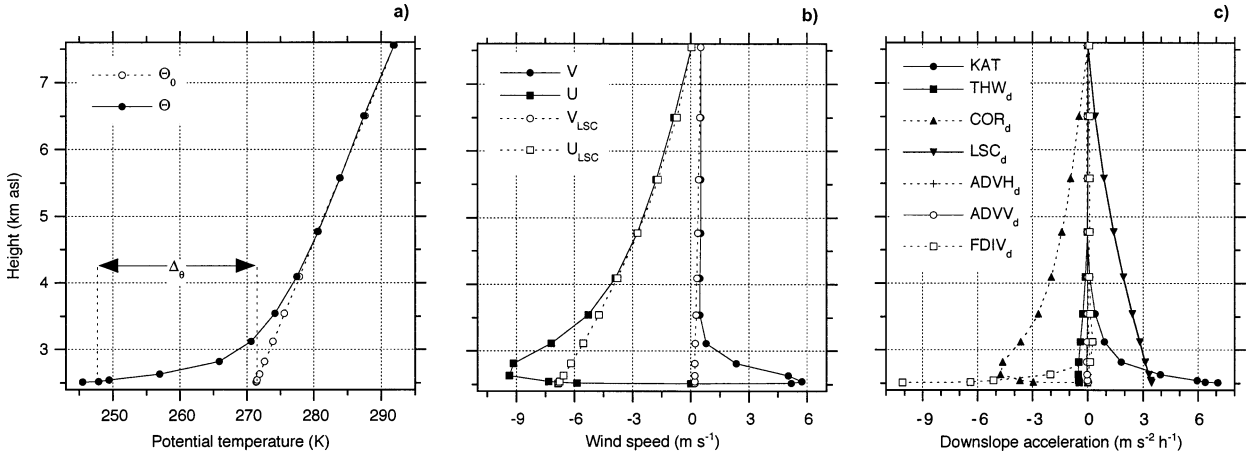

FIG. 3. Average Jul (1980–93) vertical profiles of (a) potential temperature θ and extrapolated background potential temperature θ_0 (dashed line) and SL potential temperature perturbation Δ_θ (arrow); (b) cross-and downslope wind components (U, V) and large-scale wind ($U_{\rm LSC}$, $V_{\rm LSC}$); (c) downslope momentum budget. Profiles represent avg for middle escarpment in East Antarctica (2250–2750 m MSL).

cross-slope accelerations, respectively. KAT is the katabatic pressure gradient force resulting from a negative temperature perturbation over sloping terrain; LSC represents the large-scale PGF that drives motion in the Ekman layer over flat terrain; THW represents the PGF due to horizontal changes in $\hat{\theta}$: this term drives seabreeze and snow breeze circulations over flat terrain. Horizontal and vertical advection of momentum (ADVH, ADVV) are usually small in Antarctic katabatic winds (Parish and Waight 1987). Finally, COR indicates Coriolis deflection of the flow and FDIV the vertical divergence of the turbulent momentum flux (FDIV).

b. Calculation of the terms

We assume a linear background potential temperature profile. This means that the lapse rate γ_θ of background potential temperature θ_0 is constant with height in the free troposphere:

$$\theta_0(z) = \theta_0(0) + \gamma_\theta z. \tag{3}$$

Here, θ_0 in the SL is then obtained by downward extrapolation of the free troposphere potential temperature to the surface. From that follows Δ_θ which allows the direct calculation of KAT and THW.

To calculate LSC in the SL we assume the large-scale wind ($U_{\rm LSC}$, $V_{\rm LSC}$) to be in thermal wind balance with θ_0:

$$\frac{\partial U_{\rm LSC}}{\partial \ln p} = +\frac{R_d}{f}\left(\frac{p}{p_0}\right)^{R_d/c_p}\frac{\partial \theta_0}{\partial y}$$

$$\frac{\partial V_{\rm LSC}}{\partial \ln p} = -\frac{R_d}{f}\left(\frac{p}{p_0}\right)^{R_d/c_p}\frac{\partial \theta_0}{\partial x}. \tag{4}$$

This is used to extrapolate the geostrophic wind above the TDL downwards to the SL level. The large-scale wind field ($U_{\rm LSC}$, $V_{\rm LSC}$) thus obtained directly gives us the components of LSC in Eq. (2) through multiplication by the Coriolis parameter f. The divergence of momentum flux FDIV is calculated as a residual term and absorbs model horizontal diffusion and gravity wave drag.

At this stage it is important to note that ($U_{\rm LSC}$, $V_{\rm LSC}$) is in geostrophic balance with θ_0, not with θ. This means that ($U_{\rm LSC}$, $V_{\rm LSC}$) equals the geostrophic wind only above the TDL, not in the TDL/SL. To that end we define the equivalent geostrophic wind as the stationary SL wind vector that would result from a balance of the force under consideration with the Coriolis force.

c. An example with vertical profile

Figure 3, taken from van den Broeke et al. (2002), shows an example of the calculation procedure and puts the SL results in a vertical perspective. These profiles are for July, for the middle escarpment region in East Antarctica [defined in van den Broeke et al. (2002) as the mean of all grid points in the 2250–2750-m MSL elevation interval]. This region is characterized by strong large-scale forcing. Figure 3a shows the potential temperature profile and θ_0 resulting from the extrapolation procedure. Note that the lowest point in the graph represents the surface and the first point above it the SL. The surface is 3 K colder than the SL, which is located 6–7 m above the ground. These very steep vertical temperature gradients are typical for Antarctic wintertime conditions away from the coastal regions; Δ_θ in the SL (indicated by the arrow) equals approximately −23 K.

Figure 3b shows the downslope (V, $V_{\rm LSC}$) and cross-slope (U, $U_{\rm LSC}$) wind components. A sharp maximum is visible that is characteristic of katabatic winds. The downslope component, caused by surface drag, is confined to a shallow layer below the wind speed maximum,

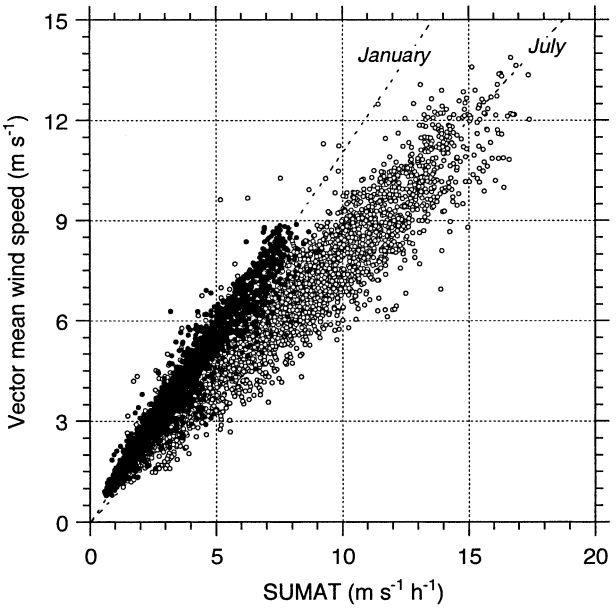

FIG. 4. Average vector mean surface layer wind speed (1980–93) as a function of the sum of active forcing terms (see text) for Jul (open dots) and Jan (black dots).

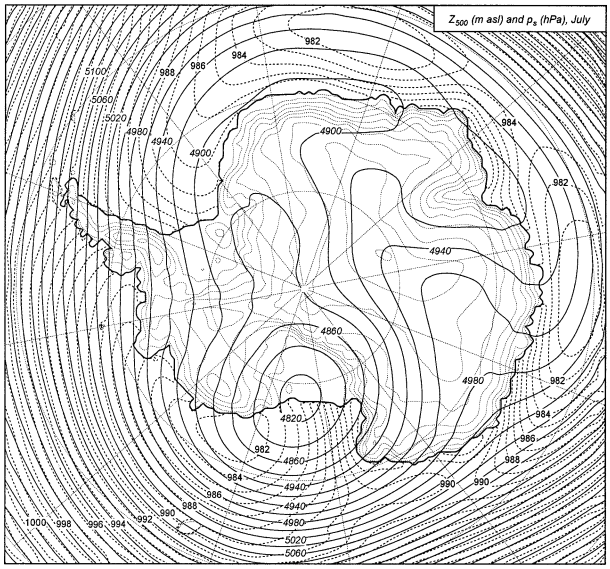

FIG. 5. Average Jul (1980–93) 500-hPa height Z_{500} (m MSL; solid contours, italic labels) and surface pressure p_s (dashed contours, over ocean only).

at which level the momentum flux divergence becomes small. Note the substantial contribution of U_{LSC} to U. In contrast, V_{LSC} is nearly zero which means that LSC acts almost entirely in the downslope direction.

The downslope momentum budget is shown in Fig. 3c. In the SL, KAT dominates in the positive downslope direction (65%) followed by LSC_d (35%). Opposing forces are THW_d (5%), COR_d (30%), and drag (FDIV_d, 65%). Naturally, drag will always be an important decelerating force in the SL because of the proximity of the surface. Note how quickly KAT decreases with height: at 1000-m height, its contribution to the downslope momentum budget is reduced to 15%.

d. Active terms in the momentum budget

In this paper, special attention is given to the relative importance of the active forces KAT, LSC, THW, ADVH, and ADVV. That is because the vector mean of the sum of these terms,

$$|\mathrm{SUMAT}| = |\mathrm{KAT} + \mathrm{LSC} + \mathrm{THW} + \mathrm{ADVH} + \mathrm{ADVV}|, \quad (5)$$

is an excellent predictor for vector mean SL wind speed (Fig. 4), with correlation coefficients of 0.94 and 0.97 for July and January, respectively. In the following we present the absolute magnitude of the individual active forces in the SL as background colors. The equivalent geostrophic wind is plotted as arrows in the foreground. These directly give the contribution of the force to the SL wind field and implicitly the direction of the force (turned 90° to the left). COR and FDIV can be regarded as passive forces, that is, they come into play only once motion has been initiated.

4. Results: July

a. LSC

SL winds in Fig. 2 are clearly more uniformly distributed than would be the case if they were driven by KAT alone. This smoothing effect at horizontal length scales of typically hundreds of kilometers is brought about by LSC that varies on much larger spatial scales than the topographically induced KAT. According to the extrapolation procedure described in section 3b, the SL large-scale wind in the SL [and thus LSC in Eq. (1)] is a function of

1) THE STRENGTH AND DIRECTION OF THE FLOW ABOVE THE TDL

Figure 5 shows the height of the 500-hPa level Z_{500} (in m MSL, solid lines) and surface pressure p_s (hPa, dashed contours, only over sea). The 500-hPa level is chosen here because it is the first standard pressure level that does not intersect with the ice sheet surface and that lies above the TDL. North of Antarctica the 500-hPa level slopes strongly poleward, forcing strong upper-air westerlies (the polar vortex). The symmetry around the pole is broken by the East Antarctic ice sheet, which introduces direct cooling of the middle troposphere, thus creating a local ''high'' pressure area at 500 hPa over the interior of East Antarctica. A minimum in Z_{500} is found over the Ross Ice Shelf (RIS), which combines a southerly location with low surface elevation.

A belt of minimum surface pressure (the circumpolar

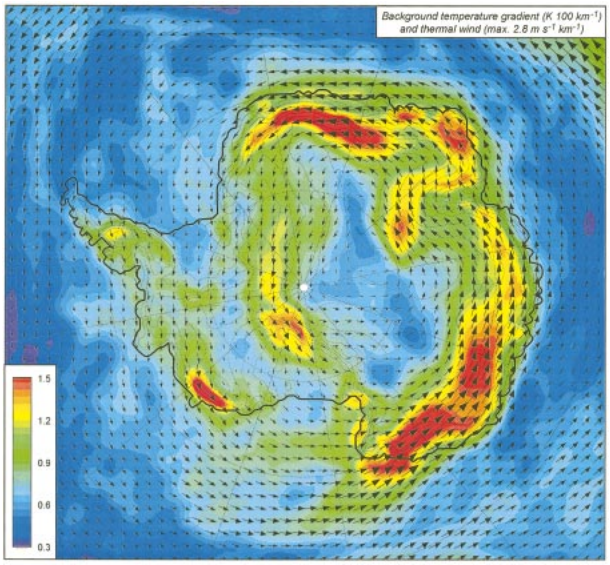

FIG. 6. Average Jul (1980–93) horizontal gradient of θ_0 (K per 100 km; colors) and associated thermal wind (m s^{-1} km^{-1}; arrows).

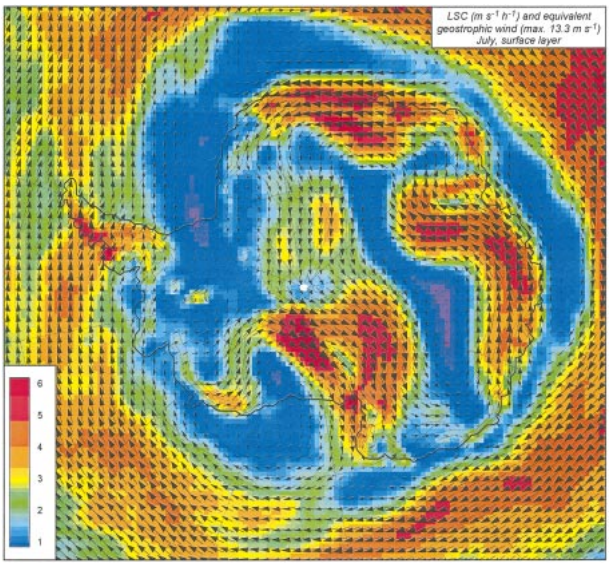

FIG. 7. Average Jul (1980–93) SL large-scale pressure gradient force LSC (m s^{-1} h^{-1}; colors) and equivalent geostrophic wind (U_{LSC}, V_{LSC}).

pressure trough) is situated just north of the Antarctic coastline. Given the local minimum of surface pressure north of Antarctica and the isobars that run broadly parallel to the height contours of the ice sheet, we expect LSC to act in the downslope direction over coastal Antarctica, along with KAT. Important deviations from zonal symmetry occur within the CPT: climatological low pressure areas are situated in those regions where the 500-hPa circulation has a significant onshore component, that is, around longitudes 20°E, 110°E, and 140°W (Fig. 5). In these regions, depressions are frequently steered towards the ice sheet by the large-scale circulation and the large-scale PGF is enhanced.

2) THE HORIZONTAL GRADIENT OF THE BACKGROUND POTENTIAL TEMPERATURE

Figure 6 shows the horizontal gradient of θ_0 in the SL (colors, in K per 100 km). This gradient is calculated from the height of the surface layer z_{SL}, θ_0, and γ_θ:

$$(\nabla_h \theta_0)_{SL} = (\nabla_h \theta_0)_{z=0} + z_{SL}(\nabla_h \gamma_\theta). \quad (6)$$

A band several hundreds kilometers wide of large θ_0 gradients roughly follows the 2000-m MSL height contour in East Antarctica. The arrows in Fig. 6 are the thermal wind vectors resulting from the horizontal gradient of θ_0 (m s^{-1} km^{-1}). They imply eastward turning of the large-scale winds in response to south–north temperature gradients, and large-scale westerlies in the upper troposphere become near-surface easterlies over the ice sheet and a strip of ocean south of the CPT (Fig. 3b).

The thermal wind vectors in Fig. 6 run along the ice sheet elevation contours. The clear connection of θ_0 gradients, representing free atmosphere conditions, with the ice sheet topography demonstrates that the cooling effect of the ice sheet is not limited to the TDL but extends far into the troposphere. In the neighborhood of the large ice shelves and over West Antarctica, the temperature gradients are weaker, with the exception of a small area in coastal West Antarctica. Over the interior of the West and East Antarctic ice sheets, the gradients are also small.

Figure 7 shows the large-scale horizontal wind vector (U_{LSC}, V_{LSC}) in the SL. It again closely follows the ice sheet contour lines, once more underlining the importance of the ice sheet topography in shaping the large-scale circulation pattern near the surface. Three regions in East Antarctica experience $|\mathbf{V}_{LSC}|$ in excess of 10 m s^{-1}:

- the southwest coast of the Ross Ice Shelf and the adjacent plateau region,
- Wilkes Land and the Lambert Glacier basin between 60° and 120°E, and
- coastal Dronning Maud Land between 0° and 45°E.

This offers an explanation for the strong SL winds that are observed on the plateau in Wilkes Land, in spite of the modest surface slope (Allison et al. 1993). The large-scale wind pattern also explains the persistent flow over the Ross Ice Shelf along the foot of the Transantarctic Mountains (Breckenridge et al. 1993). Regions with moderately strong large-scale winds are coastal west Antarctica between 120° and 150°W and the ridge of the Antarctic Peninsula, which lies in the path of strong westerlies. The Filchner–Ronne ice shelf and the eastern coast of the Weddell Sea experience weak large-scale winds.

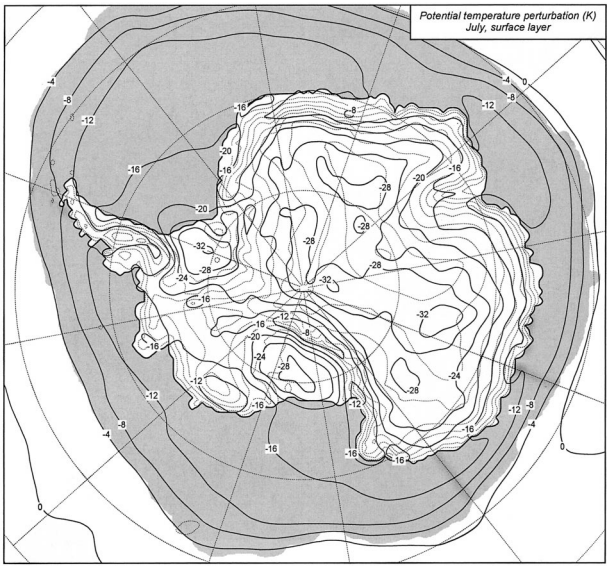

FIG. 8. Average Jul (1980–93) SL potential temperature perturbation Δ_θ (K).

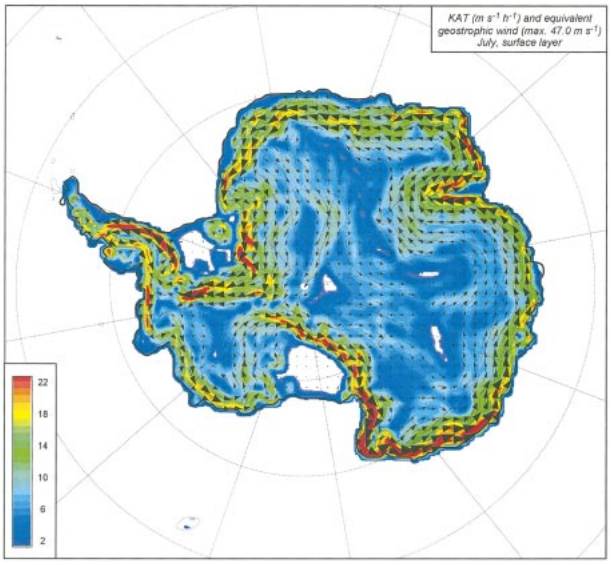

FIG. 9. Average Jul (1980–93) SL katabatic pressure gradient force KAT (m s^{-1} h^{-1}; colors) and equivalent geostrophic wind (arrows).

b. KAT

Figure 8 shows the average SL potential temperature perturbation Δ_θ for July; Δ_θ is as low as −30 K over the flat ice shelves and the interior plateau. These values are lower than the values presented by Parish and Cassano (2001) by up to 7 K. The difference may be partly caused by the slight cold bias of RACMO in the winter (typically 2–3 K; van Lipzig 1999).

Over the steeper coastal slopes, a deficit of 15–25 K is typically found, but values as high as −8 K are found in the Transantarctic Mountains and in parts of Dronning Maud Land. These maxima are probably partly artificial, aided by the exaggerated model roughness in these areas. However, 10-m snow temperatures in Dronning Maud Land do support the existence of a maximum in annual mean surface potential temperature in the escarpment region (van den Broeke et al. 1999). A feature that is not well resolved by the model is a warm band over the RIS at the foot of the Transantarctic Mountains, a region of preferred katabatic outflow and enhanced vertical mixing (Bromwich 1989b). The model places the region of enhanced mixing over the Transantarctic Mountains, likely a result of the overestimated turbulent exchange in that region.

A notable feature in Fig. 8 are the low values of Δ_θ found over the steep coastal slopes of Adélie Land, the region where the strongest katabatic winds on Earth are found. Values of −20 K occur at elevations as low as 1000 m MSL, while in other parts in East Antarctica this contour is usually found around 3000 m MSL. We speculate that the southerly large-scale winds between Adélie Land and the South Pole are responsible for this (Fig. 7). This flow pattern is made possible by the exceptional southerly location of the 500-hPa cyclonic circulation center over the Ross Ice Shelf (Fig. 5) that ensures a continuous supply of cold air to Adélie Land.

Figure 9 presents KAT (colors, m s^{-1} h^{-1}) and the equivalent geostrophic wind (arrows). According to Eq. (2), KAT depends linearly on Δ_θ multiplied by the magnitude of the surface slope. On the model grid with 55-km resolution, the surface slope increases by about one order of magnitude from the interior toward the coast, which clearly exceeds the coastward relative *decrease* of Δ_θ (Fig. 8), which does not exceed a factor of 3 to 4. As a result, KAT quickly increases toward the coast, and the highest values are found in a relatively narrow band over the steepest coastal slopes. Apart from this large-scale pattern, many small-scale features are discernible. A small but significant KAT is present over the narrow ice shelves fringing the coast of Droning Maud Land, in spite of the small surface slope of typically 1/1000. This agrees with observations from coastal stations that are situated on the shelves (Kottmeier 1986; King 1993).

In coastal Adélie Land, values of KAT exceed 20 m s^{-1} h^{-1} (Fig. 9), with an equivalent geostrophic wind speed over 40 m s^{-1}. Although SL wind speeds of this strength do occur regularly in this area, the modeled monthly mean wind speed for July is between 15 and 20 m s^{-1} (Fig. 2). Apart from surface drag, there must be another effective decelerating mechanism in the coastal area that prevents such strong winds to occur continuously, which is the topic of the next section.

c. THW

The role of THW in the momentum budget of the Antarctic SL was discussed previously by Kodama and Wendler (1986) and Pettré et al. (1993). Evidently, THW

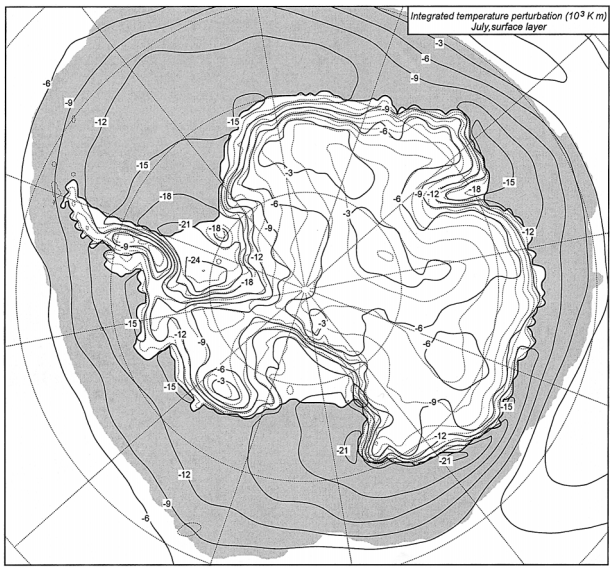

FIG. 10. Average Jul (1980–93) vertically integrated potential temperature perturbation $\hat{\theta}$ (10^3 K m).

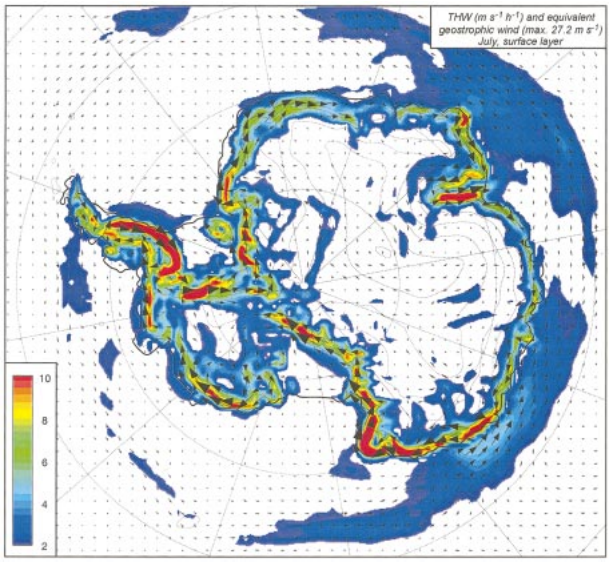

FIG. 11. Average Jul (1980–93) SL thermal wind pressure gradient force THW (m s^{-1} h^{-1}; colors) and equivalent geostrophic wind (arrows).

becomes important in areas with large horizontal gradients of $\hat{\theta}$. Figure 10 shows the average July distribution of $\hat{\theta}$ (units 1000 K m). Several interesting features show up:

- The lowest values of $\hat{\theta}$ are found over the Ross, Filchner–Ronne, and Améry Ice Shelves. These flat ice shelves act as collectors of the cold air that originates from the plateau. Strongly negative values are also found over the coastal seas where the large-scale forcing is weak (coastal Adélie Land, Enderby Land).
- The value $\hat{\theta}$ becomes more negative from interior to coast.
- There is a marked asymmetry in $\hat{\theta}$ in East Antarctica, with less negative values found in Dronning Maud Land, over the major ice ridge and the western half of Wilkes Land, and more negative values farther to the east.
- A secondary effect over the East Antarctic ice sheet is that $\hat{\theta}$ is more negative in areas that are situated eastward of large-scale promontories in the topography (e.g., Adélie Land, eastern Wilkes Land, Enderby Land), where katabatic winds converge owing to rotational effects and cold air collects.

Figure 11 presents the magnitude of THW (colors, m s^{-1} h^{-1}) and the equivalent geostrophic wind (arrows). Over the coastal ice sheet, THW has a significant magnitude that frequently exceeds 10 m s^{-1} h^{-1} and therewith becomes equally important as FDIV in the SL (not shown). This is remarkable, given the proximity of the surface.

In some coastal areas, THW effectively prevents the drainage of cold plateau air, which then becomes ''trapped'' over the ice sheet slopes. This offers a possible explanation for the sudden onset and cessation of katabatic winds in coastal East Antarctica: when the cold air over the adjacent sea ice is removed (for instance by a change in large-scale winds), the cold air over the slopes can drain to sea level. Supportive evidence must come from time series analysis of the regional momentum budget, a topic for future study. Note that the outflow of cold ice sheet air over the sea ice/ocean enhances the large-scale easterlies south of the CPT center and opposes the westerlies north of it (Fig. 11).

It must be noted that, by defining KAT and THW_d separately as in [Eq. (2)], we allow for the situation that both terms are large but of opposite sign in the case of a horizontal TDL top. This becomes evident if we assume for simplicity a TDL that has a well-defined height z_{top} while Δ_θ is constant both vertically and horizontally, so that $\hat{\theta} = \Delta_\theta(z_{\mathrm{top}} - z_{\mathrm{SL}}) \cong \Delta_\theta(z_{\mathrm{top}} - z_s)$ where z_s is the surface height. The sum of THW and KAT in the downslope momentum budget reduces to

$$\begin{aligned} \mathrm{THW}_d + \mathrm{KAT} &= \frac{g}{\theta_0}\frac{\partial \hat{\theta}}{\partial y} + \frac{g}{\theta_0}\Delta_\theta\frac{\partial z_s}{\partial y} \\ &\cong \frac{g}{\theta_0}\left[\Delta_\theta\frac{\partial(z_{\mathrm{top}} - z_s)}{\partial y} + \Delta_\theta\frac{\partial z_s}{\partial y}\right] \\ &= \frac{g}{\theta_0}\Delta_\theta\frac{\partial z_{\mathrm{top}}}{\partial y}, \end{aligned} \tag{8}$$

which becomes zero for the special case of $\partial z_{\mathrm{top}}/\partial y = 0$. This occurs, for instance, when cold air originating from the ice sheet slopes engulfs islands or ice rises in otherwise flat surroundings. Examples of large, opposite KAT and THW (cf. Figs. 9 and 11) are Berkner Island, situated on the Filchner–Ronne Ice Shelf, and the regions where the Transantarctic Mountains and the Ant-

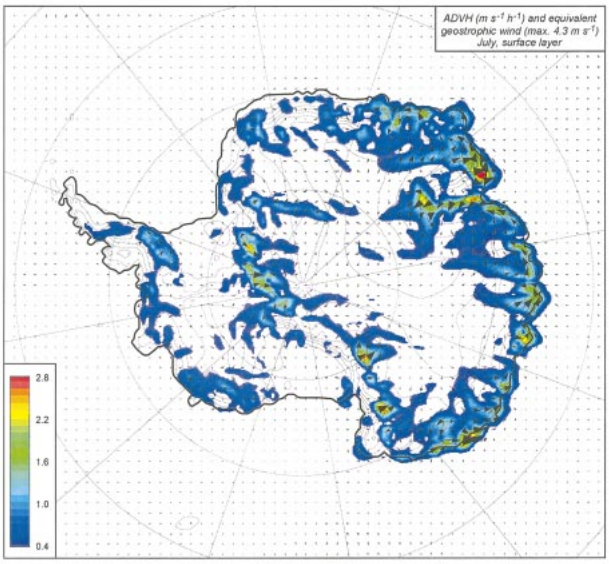

FIG. 12. Average Jul (1980–93) SL horizontal momentum advection ADVH (m s^{-1} h^{-1}; colors) and equivalent geostrophic wind (arrows).

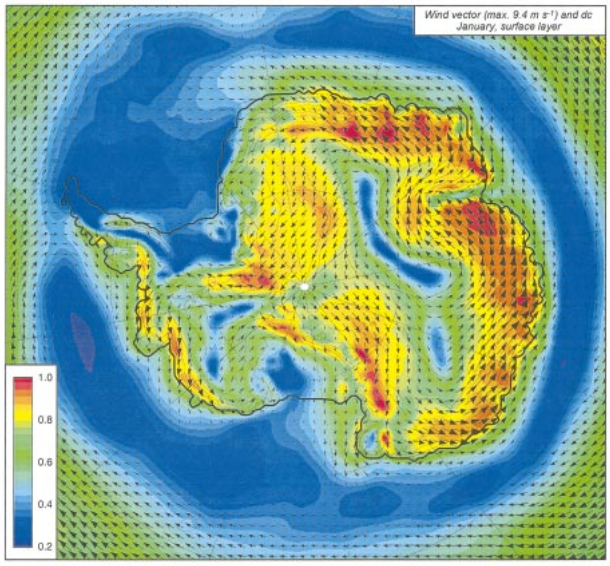

FIG. 13. Average Jan (1980–93) modeled SL wind vector (arrows) and directional constancy (colors).

arctic Peninsula border the large Ross and Filchner–Ronne Ice Shelves, respectively.

d. ADVH, ADVV

Due to the proximity of the surface, the average vertical velocity in the SL is very small and vertical advection of momentum ADVV is negligible (not shown). Horizontal momentum advection ADVH represents generally less than 10% of the SL momentum budget in idealized, two-dimensopnal topography (Parish and Waight 1987). However, its contribution to the SL downslope momentum balance is of interest, because it can both be positive and negative, and it can become important locally, especially in regions of strong topographical gradients.

Figure 12 shows the magnitude of ADVH (colors) and the equivalent geostrophic wind (arrows). The magnitude of ADVH does generally not exceed 2 m s^{-1} h^{-1}, which makes it a small term in the SL momentum budget. Because the SL flow is dominated by KAT, sudden changes in slope direction and/or magnitude are responsible for the maxima in ADVH found in the valleys of large outlet glaciers that are resolved in the RACMO/ANT1 55 km × 55 km topography. Another obvious region for ADVH to be important is the slope break, where the ice sheet terminates in the ocean; see, for instance, the strong katabatic outflow regions like Adélie Land and Enderby Land. It is important to note that ADVH may become dominant locally when model resolution is further increased. Kikuchi and Ageta (1989) argued that on spatial scales of 10 km and less, katabatic winds no longer ''feel'' slope variations, stressing the potential importance of ADVH in the SL momentum budget at resolutions much higher than the present model resolution.

5. Results: January

The January SL winds and directional constancy are presented in Fig. 13, the 500-hPa height and surface pressure in Fig. 14, and the SL large-scale wind vector in Fig. 15. Absorption of solar radiation at the surface limits the January SL Δ_θ to only a fraction of its wintertime value. KAT and THW are correspondingly

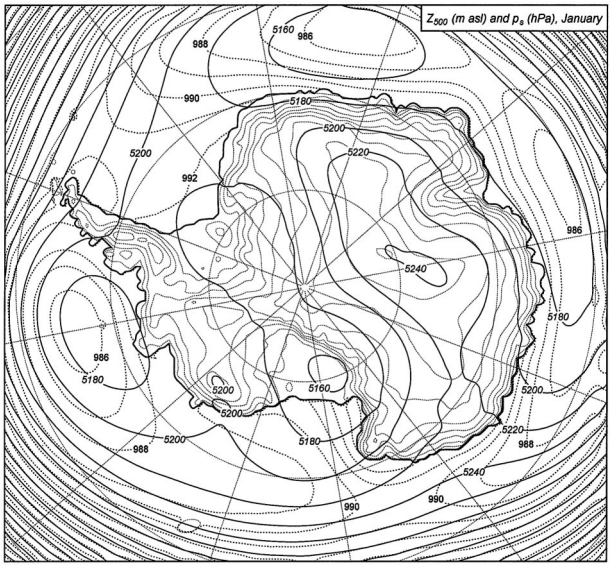

FIG. 14. Average Jan (1980–93) 500-hPa height Z_{500} (m MSL; solid contours, italic labels) and surface pressure p_s (dashed contours, over ocean only).

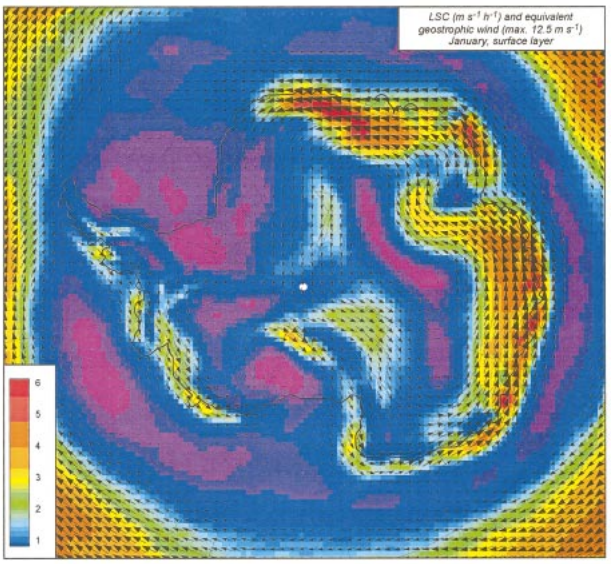

FIG. 15. Average Jan (1980–93) SL large-scale pressure gradient force LSC (m s^{-1} h^{-1}; colors) and equivalent geostrophic wind (U_{LSC}, V_{LSC}).

small, and LSC dominates the SL momentum budget. As a result, the large-scale and actual SL wind fields are very similar in strength and direction (cf. Figs. 13 and 15). As Fig. 13 shows, they still show remarkable constancy over large parts of Antarctica in spite of the weak katabatic forcing. This is in agreement with Kodama et al. (1989), who observed persistent easterly SL winds in Adélie Land in a summer meteorological experiment. The vertical wind profiles looked similar to katabatic winds but the authors demonstrated that the winds were forced largely by the large-scale pressure gradient in combination with large free-atmosphere horizontal background temperature gradients of 2 K 100 km^{-1}.

Comparing Figs. 7 and 15 reveals that SL large-scale winds are as strong in January as in July, and in some regions even stronger (e.g., in Adélie Land, eastern Wilkes Land, and Enderby Land). The greatest changes compared to July occur in coastal West Antarctica and over the Antarctic Peninsula; here, the climatological low pressure center has moved eastward from the Ross Sea towards the Bellingshausen Sea (Fig. 14). Strong large-scale easterly winds now blow along the coast of West Antarctica, while the Antarctic Peninsula experiences rather weak and variable winds from the north. The large interannual variability observed in this sector (often called the pole of variability in Antarctica) can be attributed to changes in the seasonal migration behavior of this climatological low pressure area (Cullather et al. 1996). For instance, years in which it fails to move back to the Ross Sea in winter would lead to anomalous warm conditions in the Antarctic Peninsula but colder conditions in West Antarctica (Marshall and King 1998; van den Broeke 2000).

6. Conclusions and future research

Output of the regional atmospheric climate model RACMO/ANT1 proved very suitable for the calculation of the momentum budget of the Antarctic atmospheric surface layer (SL). Regional differences in the Antarctic near-surface wind field can be explained in terms of varying relative importance of the three pressure gradient forces (PGF) in the SL, namely the katabatic PGF, the thermal wind PGF, and the large-scale PGF. In July, the katabatic PGF dominates the downslope momentum budget over the steep coastal slopes, while an opposing thermal wind PGF becomes important in a narrow band where the ice sheet meets the sea ice–covered ocean and flat ice shelves. Thermal wind effects are especially strong in areas where weak large-scale forcing allows cold air to pile up over the flat ice shelves and sea ice–covered ocean. In Wilkes Land, Dronning Maud Land, and west of the Ross Ice Shelf, the large-scale PGF forces equivalent geostrophic winds in the SL in excess of 10 m s^{-1}. Apart from the steep coastal slopes, these values are comparable in magnitude to the katabatic PGF. The large-scale PGF acts in the same direction as the katabatic PGF, that is, downslope.

In January, solar radiation reduces katabatic and thermal wind effects, and the large-scale PGF dominates the SL momentum budget. Surface layer large-scale easterly winds in some regions are stronger in summer than in winter, which explains the year-round constancy of East Antarctic SL winds. In contrast, large-scale SL winds in coastal West Antarctica and the Antarctic Peninsula are very variable on the seasonal timescale due to the shift of the climatological low pressure area in the Amundsen/Bellingshausen Sea.

For an explanation for the existing temperature (deficit) distribution over Antarctica, a similar study of the heat budget of the Antarctic near-surface air layers will be made. Future research will also focus on the annual cycle and the interannual variability of the near-surface momentum budget. Case studies are planned of exceptional regional wind regimes, such as those found in Adélie Land and Victoria Land (Bromwich 1989a). An integration with a similar model at higher horizontal and vertical resolution (RACMO/ANT2) and for a longer period (1958–present using ERA-40) is presently ongoing.

Acknowledgments. Erik van Meijgaard is thanked for supervising the runs with RACMO/ANT. We thank two anonymous reviewers for constructive comments. This work is a contribution to the European Project for Ice Coring in Antarctica (EPICA), a joint ESF (European Science Foundation)/EC scientific program, funded by the European Commission and by national contributions from Belgium, Denmark, France, Germany, Italy, the Netherlands, Norway, Sweden, Switzerland, and the United Kingdom.

REFERENCES

Allison, I., G. Wendler, and U. Radok, 1993: Climatology of the East Antarctic ice sheet (100°E to 140°E) derived from automatic weather stations. *J. Geophys. Res.,* **98** (D5), 8815–8823.

Ball, F. K., 1960: Winds on the ice slopes of Antarctica. *Antarctic Meteorology: Proceedings of the Symposium, Melbourne 1959,* Pergamon, 9–16.

Breckenridge, C. J., U. Radok, C. R. Stearns, and D. H. Bromwich, 1993: Katabatic winds along the Transantarctic Mountains. *Antarctic Meteorology and Climatology: Studies Based on Automatic Weather Stations*. D. H. Bromwich and C. R. Stearns, Eds., Antarctic Research Series, Vol. 61, 69–92.

Bromwich, D. H., 1989a: An extraordinary katabatic wind regime at Terra Nova Bay, Antarctica. *Mon. Wea. Rev.,* **117,** 688–695.

——, 1989b: Satellite analyses of Antarctic katabatic wind behavior. *Bull. Amer. Meteor. Soc.,* **70,** 738–749.

——, and Y. Du, 1994: Numerical simulation of winter katabatic winds from West Antarctica crossing Siple Coast and the Ross Ice Shelf. *Mon. Wea. Rev.,* **122,** 1417–1435.

——, and Z. Liu, 1996: An observational study of the katabatic wind confluence zone near Siple Coast, West Antarctica. *Mon. Wea. Rev.,* **124,** 462–477.

Connolley, W. M., 1996: The Antarctic temperature inversion. *Int. J. Climatol.,* **16,** 1333–1342.

Cullather, R. I., D. H. Bromwich, and M. L. van Woert, 1996: Interannual variations in Antarctic precipitation related to El Niño–Southern Oscillation. *J. Geophys. Res.,* **101,** 19 109–19 118.

Egger, J., 1985: Slope winds and the axisymmetric circulation over Antarctica. *J. Atmos. Sci.,* **42,** 1859–1867.

Gallée, H., and G. Schayes, 1992: Dynamical aspects of katabatic winds evolution in the Antarctic coastal zone. *Bound.-Layer Meteor.,* **59,** 141–161.

——, P. Pettré, and G. Schayes, 1996: Sudden cessation of katabatic winds in Adélie Land, Antarctica. *J. Appl. Meteorol.,* **35,** 1129–1141.

Genthon, C., and A. Braun, 1995: ECMWF analysis and predictions of the surface climate of Greenland and Antarctica. *J. Climate,* **8,** 2324–2332.

Hines, K. M., D. H. Bromwich, and T. R. Parish, 1995: A mesoscale modeling study of the atmospheric circulation of high southern latitudes. *Mon. Wea. Rev.,* **123,** 1146–1165.

James, I. A., 1989: The Antarctic drainage flow: Implications for hemispheric flow on the Southern Hemisphere. *Antarct. Sci.,* **1,** 279–290.

Kikuchi, T., and Y. Ageta, 1989: A preliminary estimate of inertia effects in a bulk model of katabatic wind. *Proc. NIPR Symp. Polar Meteor. Glaciol.,* **2,** 61–69.

King, J. C., 1993: Control of near-surface winds over an Antarctic ice shelf. *J. Geophys Res.,* **98,** 12 949–12 953.

Kodama, Y., and G. Wendler, 1986: Wind and temperature regime along the slope of Adélie Land, Antarctica. *J. Geophys. Res.,* **91,** 6735–6741.

——, ——, and N. Ishikawa, 1989: The diurnal variation of the boundary layer in summer in Adélie Land, eastern Antarctica. *J. Appl. Meteor.,* **28,** 16–24.

Kottmeier, C., 1986: Shallow gravity flows over the Ekström Ice Shelf. *Bound.-Layer Meteor.,* **35,** 1–20.

Mahrt, L., 1982: Momentum balance of gravity flow. *J. Atmos. Sci.,* **39,** 2701–2711.

Marshall, G. J., and J. C. King, 1998: Southern Hemisphere circulation anomalies associated with extreme Antarctic Peninsula winter temperatures. *Geophys. Res. Lett.,* **25,** 2437–2440.

Parish, T. R., 1992: On the role of Antarctic katabatic winds in forcing large-scale tropospheric motions. *J. Atmos. Sci.,* **49,** 1374–1385.

——, and D. H. Bromwich, 1987: The surface windfield over the Antarctic ice sheets. *Nature,* **328,** 51–54.

——, and K. T. Waight, 1987: The forcing of Antarctic katabatic winds. *Mon. Wea. Rev.,* **115,** 2214–2226.

——, and J. J. Cassano, 2001: Forcing of the wintertime Antarctic boundary layer winds from the NCEP–NCAR global reanalysis. *J. Appl. Meteor.,* **40,** 810–821.

Pettré, P., and J. C. André, 1991: Surface pressure change through Loewe's phenomena and katabatic flow jumps: Study of two cases in Adélie Land, Antarctica. *J. Atmos. Sci.,* **48,** 557–571.

——, C. Payan, and T. R. Parish, 1993: Interaction of katabatic flow with local thermal effects in a coastal region of Adélie Land, East Antarctica. *J. Geophys. Res.,* **98,** 10 429–10 440.

Phillpot, H. R., and J. W. Zillman, 1970: The surface temperature inversion over the Antarctic continent. *J. Geophys. Res.,* **75,** 4161–4169.

Schwerdtfeger, W., 1970: The climate of the Antarctic. *World Survey of Climatology,* Vol. XIV, S. Orvig, Ed., Elsevier, 253–355.

van den Broeke, M. R., 2000: On the interpretation of Antarctic temperature time series. *J. Climate,* **13,** 3885–3889.

——, and R. Bintanja, 1995: Summer time atmospheric circulation in the vicinity of a blue ice area in east Queen Maud Land, Antarctica. *Bound.-Layer Meteor.,* **72,** 411–438.

——, R. S. W. van de Wal, and M. Wild, 1997: Representation of Antarctic katabatic winds in a high resolution GCM and a note on their climate sensitivity. *J. Climate,* **10,** 3111–3130.

——, J.-G. Winther, E. Isaksson, J. F. Pinglot, L. Karlöf, T. Eiken, and L. Conrads, 1999: Climate variables along a traverse line in Dronning Maud Land, East Antarctica. *J. Glaciol.,* **45,** 295–302.

——, N. P. M. van Lipzig, E. van Meijgaard, and J. Oerlemans, 2002: Momentum budget of the East Antarctic atmospheric boundary layer: Results of a regional climate model. *J. Atmos. Sci.,* **59,** 3117–3129.

van Lipzig, N. P. M., 1999: The surface mass balance of the Antarctic ice sheet: A study with a regional atmospheric model. Ph.D. thesis, Utrecht University, 154 pp. [Available from IMAU, P.O. Box 80005, 3508 TA Utrecht, Netherlands.]

——, E. van Meijgaard, and J. Oerlemans, 1998: Evaluation of a regional atmospheric climate model for January 1993, using in situ measurements from the Antarctic. *Ann. Glaciol.,* **27,** 507–514.

——, ——, and ——, 1999: Evaluation of a regional atmospheric model using measurements of surface heat exchange processes from a site in Antarctica. *Mon. Wea. Rev.,* **127,** 1994–2011.

Weller, G., 1969: A meridional wind speed profile in Mac Robertson Land, Antarctica. *Pure Appl. Geophys.,* **77,** 193–200.